ELSEVIER

Engineering Analysis with Boundary Elements 24 (2000) 131–144

ENGINEERING ANALYSIS *with* BOUNDARY ELEMENTS

www.elsevier.com/locate/enganabound

Use of constant, linear and quadratic boundary elements in 3D wave diffraction analysis

A. Tadeu*, J. António

Department of Civil Engineering, Faculty of Science and Technology, University of Coimbra, 3030 Coimbra, Portugal

Received 8 September 1999; accepted 29 November 1999

Abstract

The performance of the Boundary Element Method (BEM) depends on the size of the elements and the interpolation function used. However, improvements in accuracy and efficiency obtained with both expansion and grid refinement increases demand on the computational effort. This paper evaluates the performance of constant, linear and quadratic elements in the analysis of the three-dimensional scattering caused by a cylindrical cavity buried in an infinite homogeneous elastic medium subjected to a point load. A circular cylindrical cavity for which analytical solutions are known is used in the simulation analysis. First, the dominant BEM errors are identified in the frequency domain and related to the natural vibration modes of the inclusion. Comparisons of BEM errors are then made for different types of boundary elements, maintaining similar computational costs. Finally, the accuracy of the BEM solution is evaluated when the nodal points are moved inside linear and quadratic discontinuous elements.

Keywords: Boundary elements; Constant; Linear and quadratic elements; Wave propagation

1. Introduction

The solution of how waves propagate between a source and a receiver placed below the ground has occupied researchers for years. Some of the first analytical studies on wave diffraction and scattering were concerned with the problem of wave motion and reverberations in alluvial basins of regular shape [1,2], and with wave scattering induced by cavities [3–6]. More recently, semi-analytical methods have been used to analyse wave diffraction caused by geological irregularities of arbitrary shape within globally homogeneous media [7–9]. By contrast, the application of purely numerical methods (i.e. finite elements or differences combined with boundaries) has been restricted, for the most part, to situations where the response is required only within localised irregular domains, such as soil–structure interaction problems [10–12]. Discrete methods have also occasionally been used to model large alluvial basins, but only in plane-strain [13]. Finally, hybrid methods involving a combination of finite elements, to model the interior domain containing the inhomogeneities, and semi-analytical representations for the exterior domain have been used [14].

The application of these numerical methods has mostly been restricted to situations where the solution is required within two-dimensional (2D) domains. The evaluation of the full scattering wave field generated by sources placed in the presence of three-dimensional (3D) propagation media requires the use of computationally demanding numerical schemes.

The solution becomes much simpler if the medium is 2D, even if the dynamic source remains 3D, a point load, for example. Such a situation is frequently referred to as a two-and-a-half-dimensional problem (2-1/2-D), for which solutions can be obtained by means of a two spatial Fourier transform in the direction in which the geometry does not vary. This requires solving a sequence of 2D problems with different spatial wavenumbers k_z. Then, using the inverse Fourier transform, the 3D field can be synthesized.

This solution is known in closed form for inclusions with simple geometry, such as a circular cylinder, for which the wave equation is separable. However, if the inclusion has an irregular cross-section it is more difficult to obtain the solution. In this case, the Boundary Element Method (BEM) is possibly the best tool for analyzing wave propagation in unbounded media, because it automatically satisfies the far-field radiation conditions and allows a compact description of the medium in terms of boundary elements placed at the material's discontinuities [15–18].

* Corresponding author. Tel.: +351-239-797202; fax: +351-239-797190.

0955-7997/00/$ - see front matter
PII: S0955-7997(99)00064-8

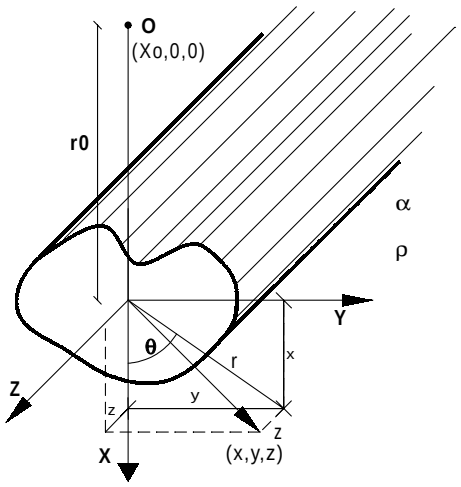

Fig. 1. Geometry of the problem.

The BEM solution at each frequency is expressed in terms of waves with varying wavenumber k_z, (with z being the direction in which the geometry does not vary), which is subsequently Fourier transformed into the spatial domain. The wavenumber transform in discrete form is obtained by considering an infinite number of virtual point sources equally spaced along the z-axis and at a sufficient distance from each other to avoid spatial contamination [19]. In addition, the analyses are performed using complex frequencies, shifting the frequency axis down, in the complex plane, in order to remove the singularities on (or near) the axis, and to minimize the influence of the neighboring fictitious sources [20].

The accuracy of the BEM solution depends on the number of the boundary elements used to discretize the material discontinuities and on the nodes inside each element [21,22]. The BEM solution improves as the order of the element increases and its size decreases. However, the improvement in accuracy and efficiency that can be obtained by using higher order elements is offset by the increased computational cost in CPU time. Thus, while the response improves with the number of nodes per element, this is not necessarily useful, because of the increased computational expense that these more accurate models entail.

The present work assesses the benefit of using constant, linear and quadratic elements to calculate the displacement field around a circular cylindrical cavity buried inside an elastic medium, for which the solution is known in closed form.

This paper first formulates the problem and briefly presents the equations required to solve the BEM problem, while its analytical solution is addressed in Appendix A. Then, the BEM errors occurring in the 3D scattering analysis of a cylindrical circular cavity are identified in the frequency domain and correlated to those related to the natural vibration modes. In these analyses, different numbers of constant, linear and quadratic elements are used, according to different ratios of the incident wave wavelength to the length of the boundary elements. Results computed with a similar number of nodal points are compared, thus keeping the computational cost essentially constant. Thereafter, the performance of discontinuous linear and quadratic elements is analyzed when the positions of the nodal points inside the boundary elements are moved around in the vicinity of those used in the Gauss–Legendre numerical integration.

2. Problem formulation

Consider a cylindrical irregular cavity of infinite extent, buried in a spatially uniform elastic medium (Fig. 1), subjected to a harmonic dilatational point source at position $(x_0, 0, 0)$, oscillating with a frequency ω. The incident field

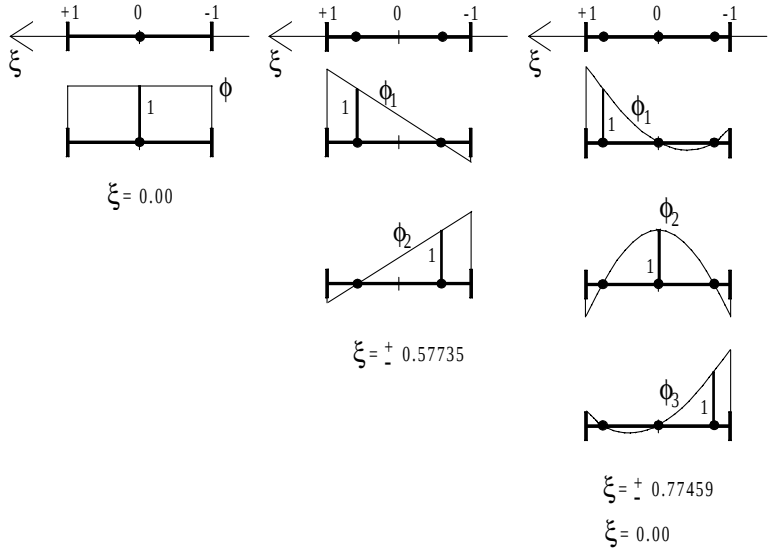

Fig. 2. Interpolation functions and position of the nodal points.

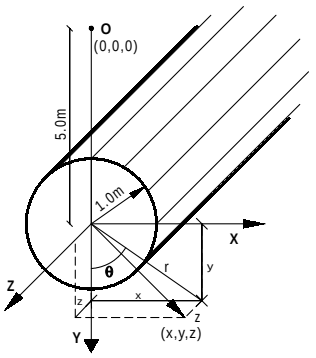

$\alpha = 4208\ m/s$

$\beta = 2656\ m/s$

$\rho = 2140\ kg/m^3$

Fig. 3. Circular cylindrical cavity in an unbounded elastic medium. Medium properties.

can be expressed by means of the now classical dilatational potential ϕ.

$$\phi_{\text{inc}} = \frac{A e^{i\frac{\omega}{\alpha}(\alpha t - \sqrt{(x-x_0)^2+y^2+z^2})}}{\sqrt{(x-x_0)^2+y^2+z^2}} \tag{1}$$

in which the subscript *inc* denotes the incident field, A is the wave amplitude, α is the compressional wave velocity of the medium, and $i = \sqrt{-1}$.

Defining the effective wavenumbers

$$k_\alpha = \sqrt{\frac{\omega^2}{\alpha^2} - k_z^2}, \qquad \text{Im } k_\alpha < 0 \tag{2}$$

by means of the axial wavenumber k_z, and Fourier-transforming Eq. (1) in the z direction, one obtains

$$\hat{\phi}_{\text{inc}}(\omega, x, y, k_z) = \frac{-iA}{2} H_0^{(2)}(k_\alpha \sqrt{(x-x_0)^2+y^2}) \tag{3}$$

in which the $H_n^{(2)}(\ldots)$ are second Hankel functions of order n.

If one considers an infinite number of virtual point sources equally spaced along the z direction at a sufficient distance, L, from each other to avoid spatial contamination [19], the incident field may be written as

$$p_{\text{inc}}(\omega, x, y, z) = \frac{2\pi}{L} \sum_{m=-\infty}^{\infty} \hat{p}_{\text{inc}}(\omega, x, y, k_z)\, e^{-ik_{zm}z} \tag{4}$$

with $k_{zm} = (2\pi/L)m$. This equation converges and can be approximated by a finite sum of terms.

3. Boundary element formulation

The BEM is used to obtain the 3D field generated by a cylindrical cavity subjected to spatially sinusoidal harmonic line loads defined by Eq. (3). The fundamental equations underlying the application of boundary elements to wave propagation are well known [23]. It is therefore enough to state here that the application of the method in the frequency domain requires for the type of scattering problem presented herein the evaluation of the integral

$$H_{il}^{kl} = \int_{C_l} \phi H_{il}(x_k, x_s, n_s)\, dC_l \qquad (i, l = 1, 2, 3) \tag{5}$$

in which $H_{il}(x_k, x_s, n_s)$ are the traction components at the point x_k in direction i caused by a concentrated load acting at the source point x_s in direction l. Also, n_s is the unit outward normal for the lth boundary segment C_l and ϕ are the interpolation functions.

Expressions for the tensions may be obtained from the 2-1/2-D *fundamental solution* G_{il}, by taking partial derivatives to deduce the strains and then applying Hooke's law to obtain the stresses. The displacement functions that apply to the present case can be written as follows:

$$G_{xx} = B_0 \Bigg\{ (-ik_z)^2 H_0^{(2)}(k_\beta r) + k_\beta^2 \times \Bigg[-H_0^{(2)}(k_\beta r) + \frac{B_1}{k_\beta r} - \frac{\partial r}{\partial x}\frac{\partial r}{\partial x} B_2 \Bigg] \Bigg\} \tag{6}$$

$$G_{yx} = G_{xy} = B_0 \Bigg[-k_\beta^2 \Big(\frac{\partial r}{\partial x}\frac{\partial r}{\partial y} B_2 \Big) \Bigg] \tag{7}$$

$$G_{zx} = G_{xz} = B_0 \Bigg[k_\beta \Big(\frac{\partial r}{\partial x} B_1 \Big) \Bigg] (-ik_z) \tag{8}$$

$$G_{yy} = B_0 \Bigg\{ (-ik_z)^2 H_0^{(2)}(k_\beta r) + k_\beta^2 \times \Bigg[-H_0^{(2)}(k_\beta r) + \frac{B_1}{k_\beta r} - \frac{\partial r}{\partial y}\frac{\partial r}{\partial y} B_2 \Bigg] \Bigg\} \tag{9}$$

$$G_{zy} = G_{yz} = B_0 \Bigg[k_\beta \Big(\frac{\partial r}{\partial y} B_1 \Big) \Bigg] (-ik_z) \tag{10}$$

$$G_{zz} = B_0 \lfloor -k_\beta^2 H_0^{(2)}(k_\beta r) + (-ik_z)^2 H_0^{(2)}(k_\alpha r) \rfloor \tag{11}$$

with $k_\beta = \sqrt{\frac{\omega^2}{\beta^2} - k_z^2}$, $r = \sqrt{x^2+y^2}$, $\xi = \frac{k_\alpha}{k_\beta}$,

$$B_0 = \frac{i}{4\rho\omega^2},\ B_n = (H_n^{(2)}(k_\beta r) - \xi^n H_n^{(2)}(k_\alpha r))$$

$n = 1, 2$

After mathematical manipulation of the integral equations, combined and subjected to the continuity conditions at the interface between the two media, and discretized appropriately, a system of equations is obtained that can be solved for the nodal displacements. The required integrations in Eq. (5) are performed using Gaussian quadrature when the element to be integrated is not the loaded element. For the loaded element, the existing singular integrands are carried out in closed form [18].

The system of equations obtained is fully populated and

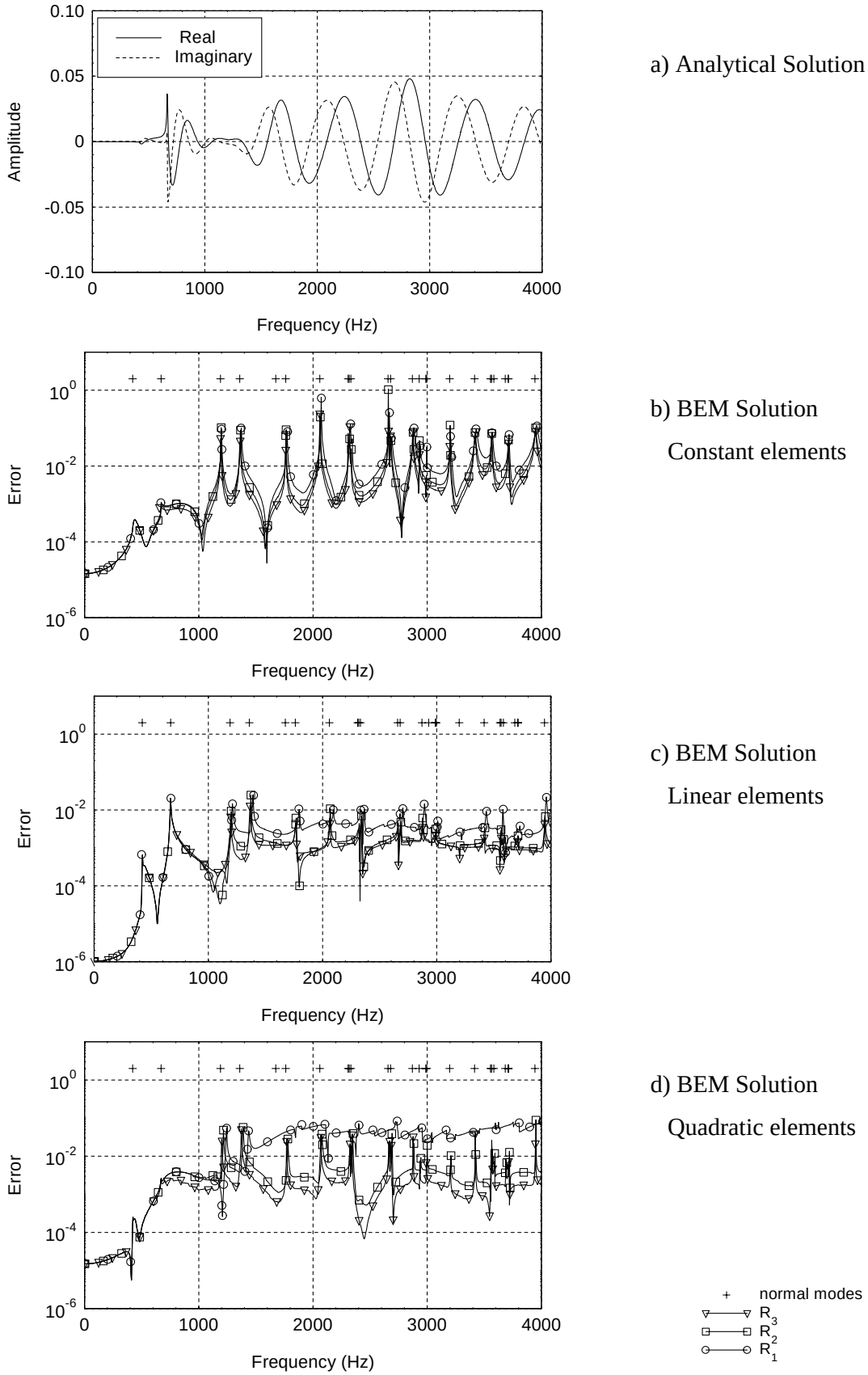

Fig. 4. Scattering response at receiver 1 ($k_z = 1$ rad/(m/s)).

Table 1
Relations λ/L used in the calculations

Interpolation function	R_1	R_2	R_3
Constant	6	12	18
Linear	3	6	9
Quadratic	2	4	6

in general not symmetric. As a consequence, the global computational cost of the BEM mainly represents the time required to solve the system of equations. In this paper, different types of boundary elements are used. The performance of the different solutions is evaluated by comparing the results obtained for similar computational cost; that is, involving equation systems of the same size (i.e. using a similar number of nodal points).

The displacement and stress variations within a boundary element are defined as a function of the nodal values. Discontinuous boundary elements are used to deal with the traction discontinuity existing at the corner between two boundary elements. This consists of moving to the inside the nodes that would meet at the corner [24]. Fig. 2 presents the interpolation functions used to model the inclusions used in the simulation analysis.

4. Analytical solution

The scattering field produced by a circular cylindrical cavity, placed in a homogeneous elastic medium, subjected to a point dilatational load can be defined in a circular cylindrical coordinate system (r, θ, z) and evaluated by

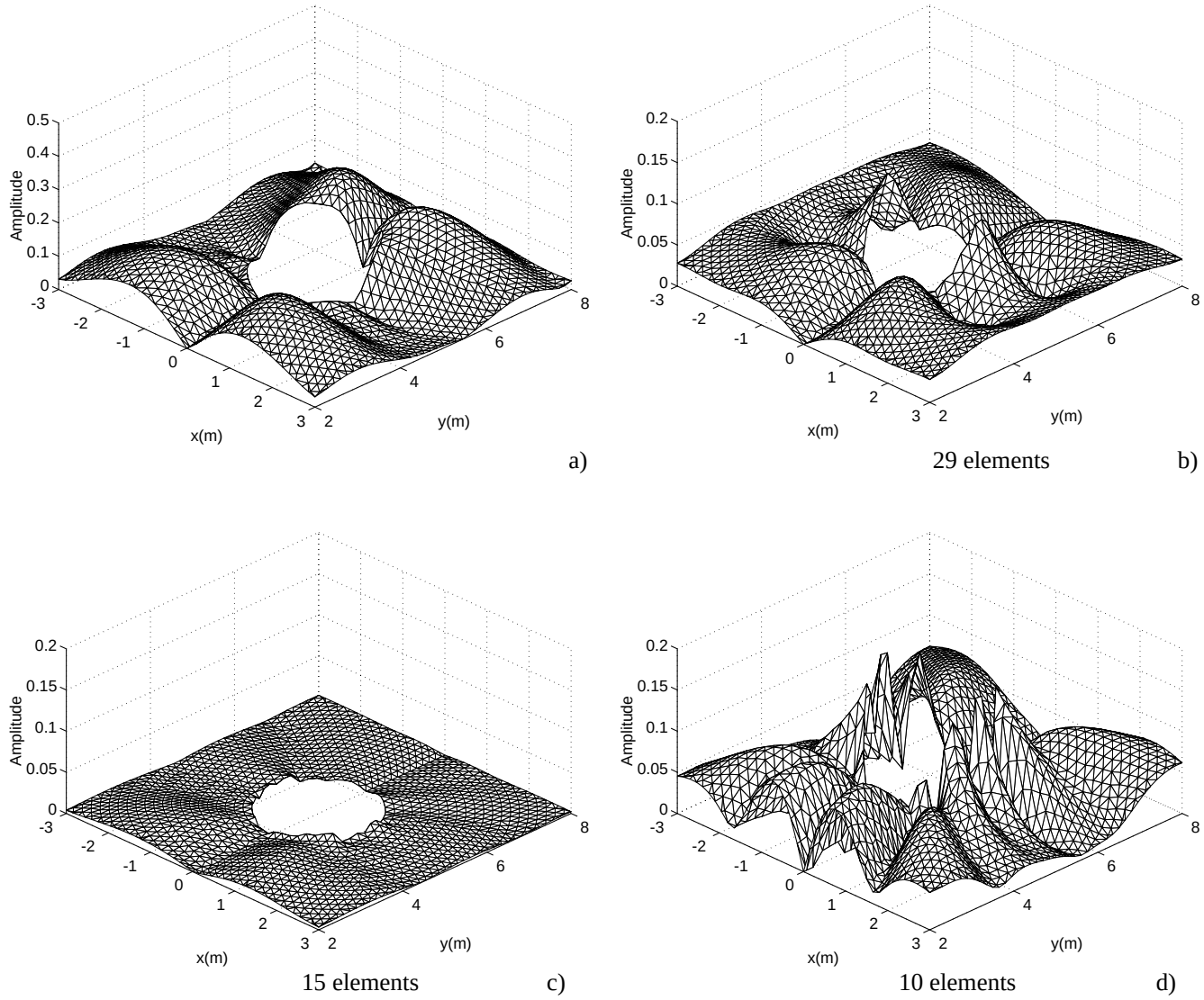

Fig. 5. Horizontal displacements ($k_z = 1$ rad/(m/s)). Frequency of excitation—2058.6 Hz: (a) analytical solution; (b) modulus of the BEM error (R_1)—constant elements; (c) modulus of the BEM error (R_1)—discontinuous linear elements; and (d) modulus of the BEM error (R_1)—discontinuous quadratic elements.

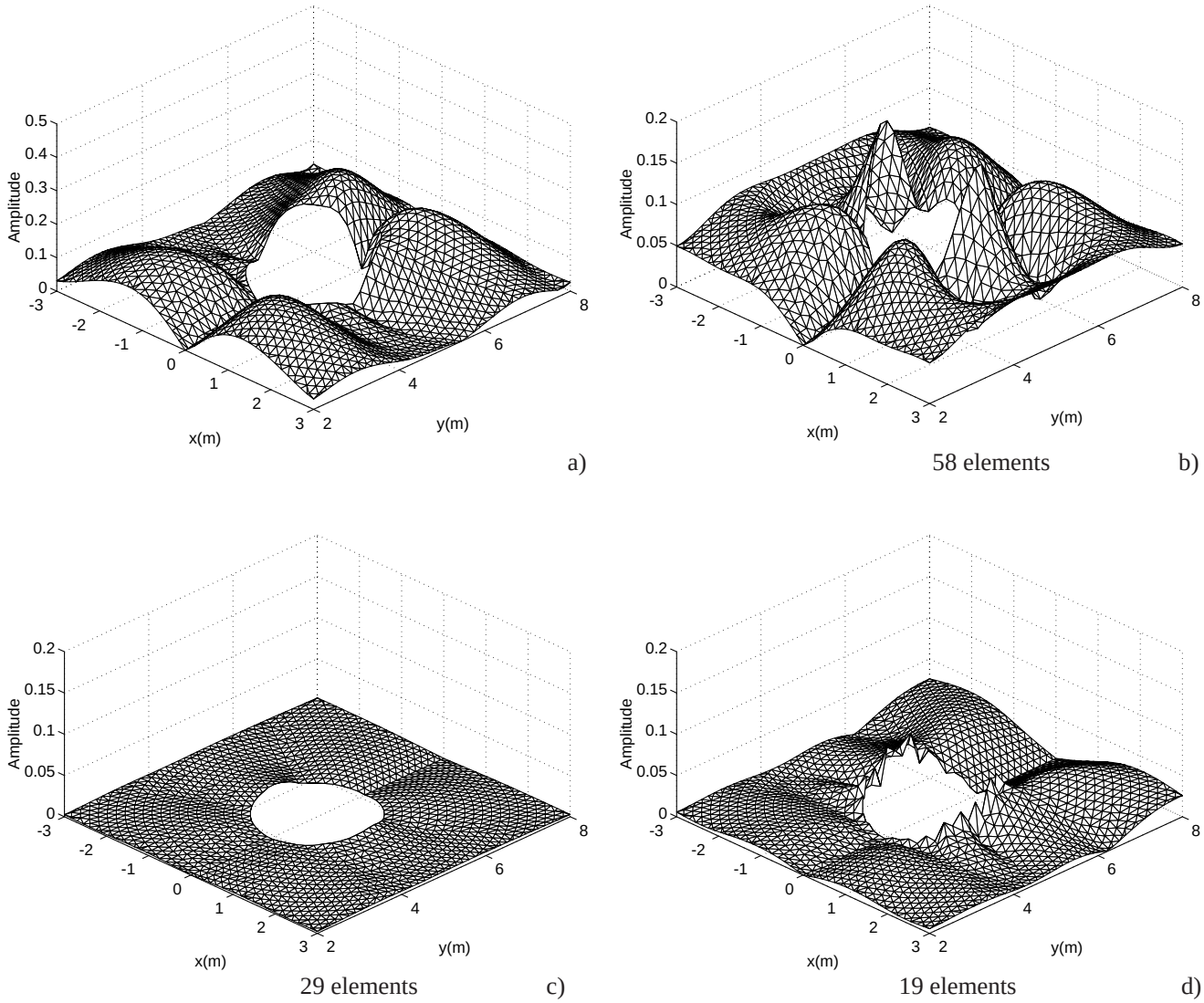

Fig. 6. Horizontal displacements ($k_z = 1$ rad/(m/s)). Frequency of excitation—2058.6 Hz: (a) analytical solution; (b) modulus of the BEM error (R_2)—constant elements; (c) modulus of the BEM error (R_2)—discontinuous linear elements; and (d) modulus of the BEM error (R_2)—discontinuous quadratic elements.

using the separation of variables method, as briefly described in Appendix A [25,26].

5. Analytical versus boundary element solution

The benefit of using higher order elements is evaluated by calculating the displacement field around a cylindrical circular cavity buried in an infinite homogeneous space. The cavity is struck by *P* waves elicited by a dilatational point load applied at point *O*, as in Fig. 3.

Simulation analyses have been performed for a broad range of frequencies and inclusions. However, given the impossibility of presenting all the results, a restricted number of simulations will be used to illustrate the main findings.

6. Position of the BEM errors in the frequency versus wavenumber domain

Fig. 4 gives some of the scattering results obtained at one receiver placed at $x = 2.5$ m and $y = 4.0$ m, hereinafter designated receiver 1. The results are computed for 1000 frequencies, in the range 4.0–4000 Hz. The response was calculated both analytically and by using the BEM, discretizing the boundary with constant, linear and quadratic discontinuous elements, as shown in Fig. 2. The positions of the nodal points are the same as those used in Gauss–Legendre numerical integration (Fig. 2). Displacements in *x*, *y* and *z* directions were computed for a wide range of wavenumbers k_z, which were then be used to obtain the 3D solution by means of (fast) inverse Fourier transform into space. To illustrate the results, only the horizontal

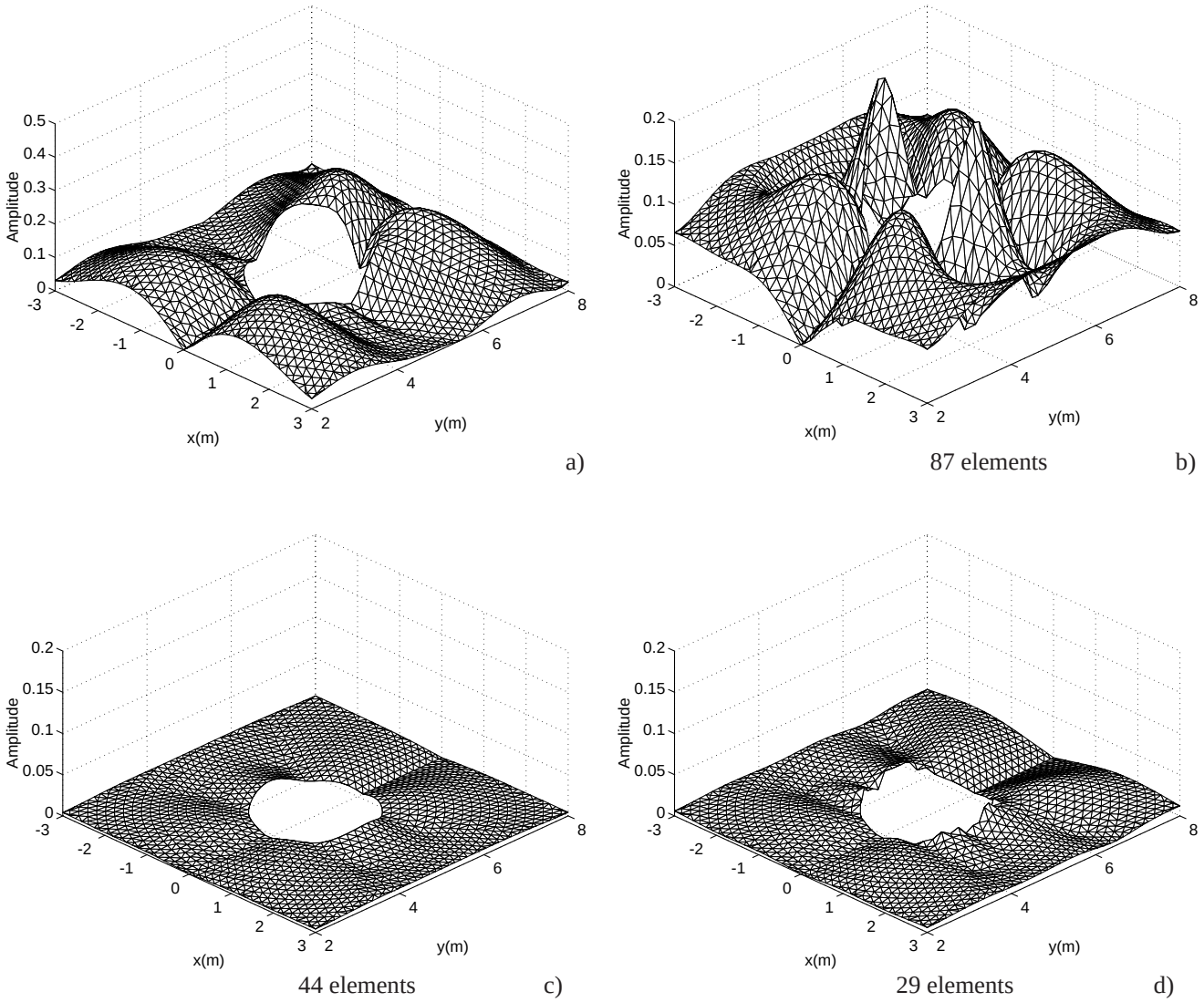

Fig. 7. Horizontal displacements ($k_z = 1$ rad/(m/s)). Frequency of excitation—2058.6 Hz: (a) analytical solution; (b) modulus of the BEM error (R_3)—constant elements; (c) modulus of the BEM error (R_3)—discontinuous linear elements; and (d) modulus of the BEM error (R_3)—discontinuous quadratic elements.

displacements for $k_z = 1.0$ rad/(m/s) will be given. Fig. 4a gives the exact values for the horizontal displacement. Fig. 4b–d, illustrate the error occurring with the BEM solution when constant, linear and quadratic elements are used. To enhance the difference in the responses the error is displayed on a logarithmic scale. Three different relations (R_1, R_2, R_3) between the wavelength (λ) of the shear waves and the length of the boundary elements (L) were considered, as listed in Table 1. In all cases, the number of the nodal points is at least 24. The positions of the lower natural modes, given by solving Eq. (A6), are also displayed.

Analysis of the results shows that the BEM accuracy is much poorer at frequencies in the vicinity of the natural modes, for which big peaks of error occur. The constant elements are conspicuously bad in these localized frequency domains. Outside these domains, all the responses improve as the number of the nodal points increases. This was predictable since an element with a greater number of nodes can approximate the response better, because it can model variations in displacement and/or traction much more realistically. It can further be observed that, as the number of boundary elements increases, the position of the error peaks moves towards the values of the frequencies satisfying Eq. (A6). This behavior can be explained by the fact that the increased number of elements allows the BEM model to approach the definition of the circular cylinder better, with respect to its dynamic behavior.

In addition, it can be observed that for higher relations of λ/L (R_2 and R_3), the BEM errors obtained, using linear and quadratic elements, have a global tendency to decrease as the frequency increases. That is to say, a better degree of accuracy is therefore expected for the higher frequencies

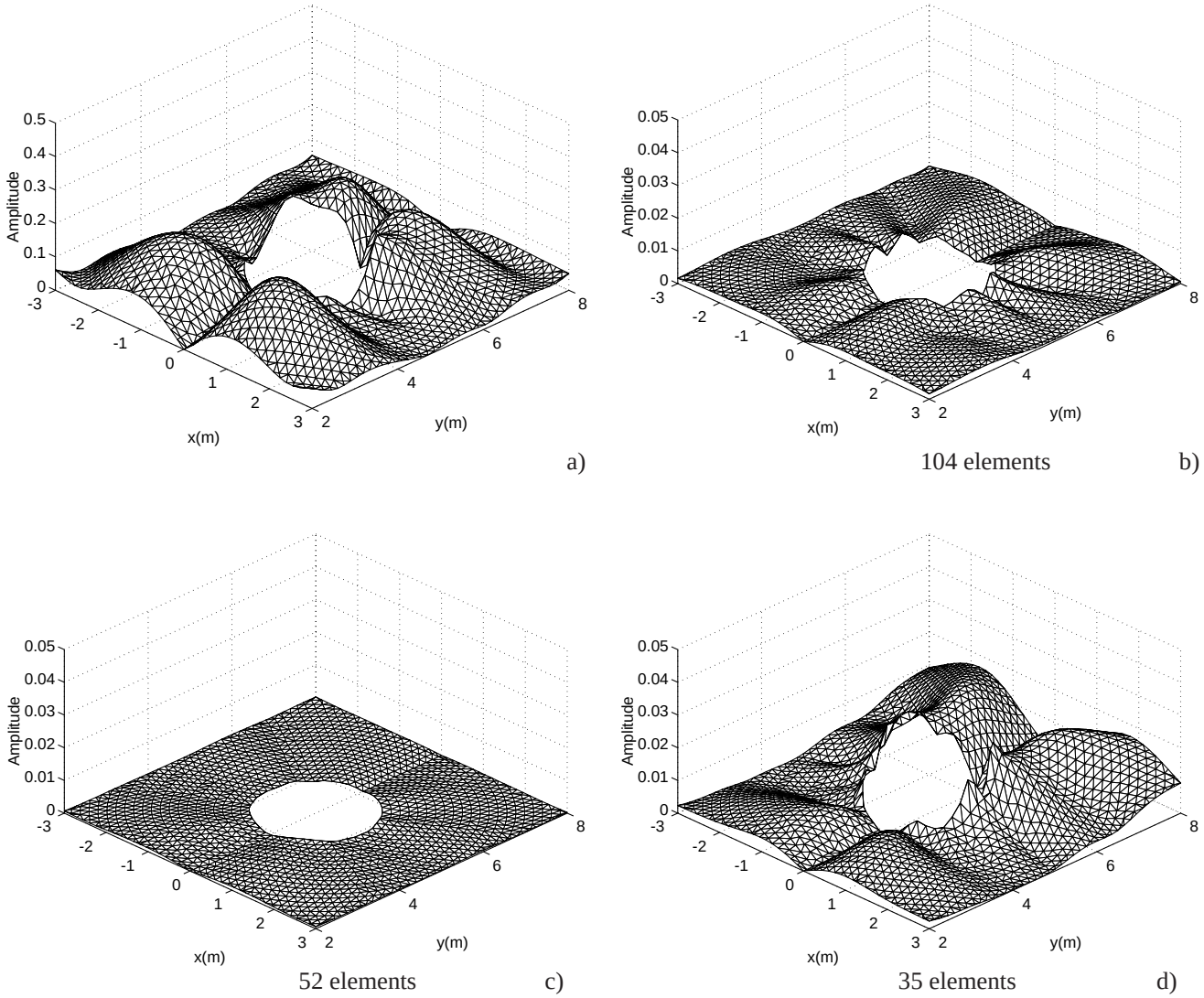

Fig. 8. Horizontal displacements ($k_z = 1$ rad/(m/s)). Frequency of excitation—2450 Hz: (a) analytical solution; (b) modulus of the BEM error (R_3)—constant elements; (c) modulus of the BEM error (R_3)—discontinuous linear elements; and (d) Modulus of the BEM error (R_3)—discontinuous quadratic elements.

because, to satisfy a specific relation of λ/L, more boundary elements are required for those excitation frequencies than for lower ones. The number of the elements itself seems to be an important factor, in addition to the number of elements required to satisfy a specific relation of λ/L.

7. Behavior of BEM solution in the vicinity of the natural modes

In order to get a better picture of the behavior of the influence of the natural modes on the BEM solution, the scattering response was subsequently calculated over a fine grid, placed around the cavity. In the following example the inclusion is struck by a pulsating source vibrating at a single frequency at $k_z = 1.0$ rad/(m/s), which is either 2058.6 or 2450 Hz. These two frequencies correspond to one of the natural modes of the real system (Eq. (A6)) and a frequency outside the vicinity of any eigen-frequency, respectively. The inclusion is modeled with discontinuous elements, using constant, linear and quadratic interpolation functions. The nodal points are not at the end of these elements, but rather shifted inside them, to allow nodal points in which only the stresses relative to the element itself to be considered.

The number of elements was chosen to allow comparison with results evaluated at similar computational cost (i.e. the same number of nodal points). In these calculations three different ratios between the wavelength of the shear waves and the length of the boundary elements were considered, as listed in Table 1.

Figs. 5–7 illustrate the analytical response and the modulus of the error occurring with the BEM solution for a frequency of 2058.6 Hz, when different relations λ/L are used (R_1,R_2, and R_3). As can be seen, the agreement between the BEM and the analytical solution is not good when constant elements are used to model the inclusion (Figs.

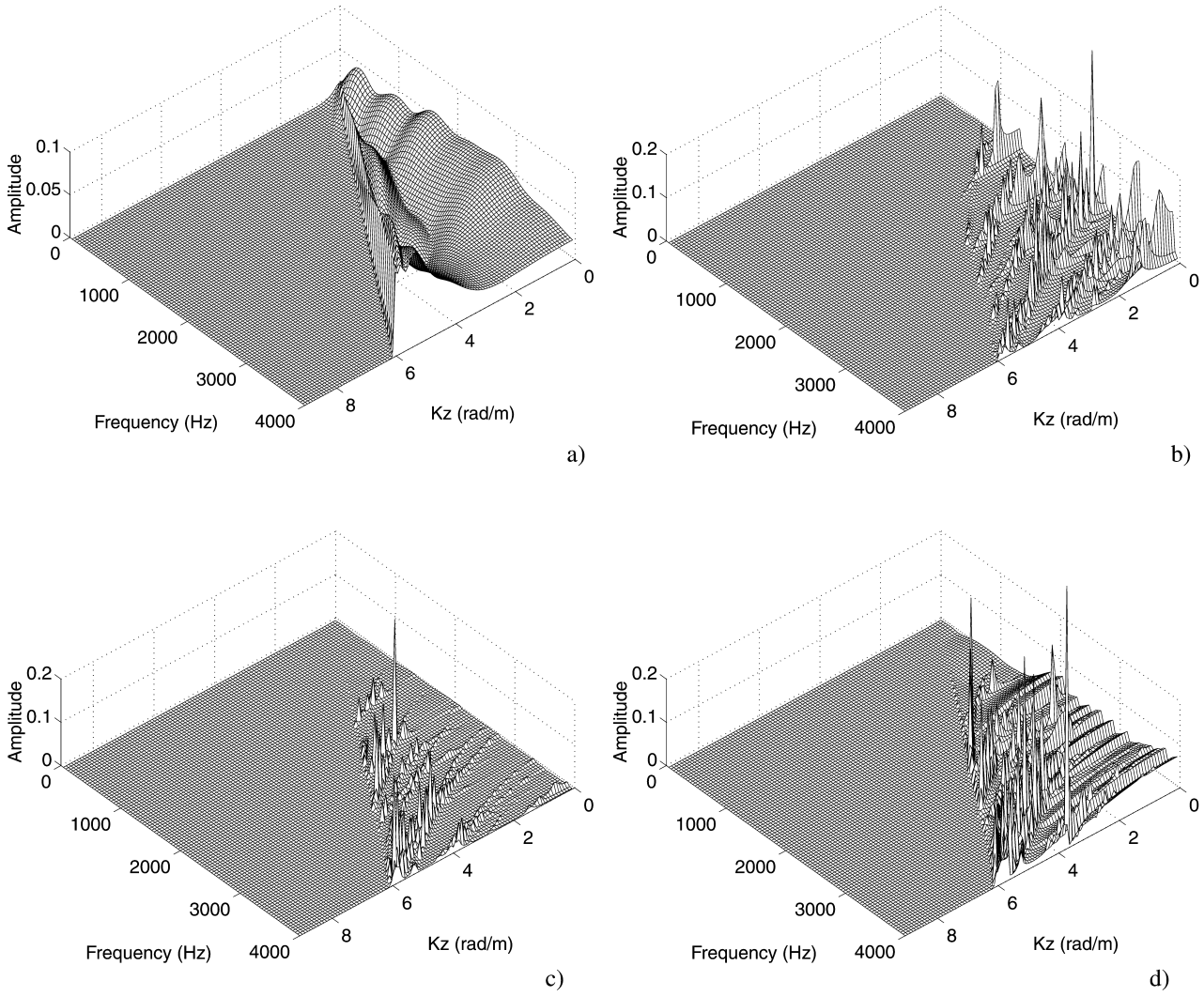

Fig. 9. Horizontal displacements at receiver 1 in the frequency versus wavenumber domain: (a) analytical solution; (b) modulus of the BEM error (R_1)—constant elements; (c) modulus of the BEM error (R_1)—discontinuous linear elements; and (d) modulus of the BEM error (R_1)—discontinuous quadratic elements.

5b, 6b and 7b). Notice that the BEM error is significant, with values similar to those given by the analytical solution. It can further be observed that the BEM solution does not improve as refinements are made to the boundary elements (i.e. changing the number of elements). Indeed, when the inclusion is modeled using 87 constant elements the error increases (see Fig. 7b). Notice that as the number of boundary elements increases, the BEM model defines the behavior of the circular inclusion better, approaching, in this case, one of its natural modes ($f = 2058.6$ Hz). As the constant boundary elements perform poorly in the vicinity of the natural modes, they cause the error to increase, because it approaches the behavior of one of the natural modes. If the number of the boundary elements is further increased (not shown here), at greater computational cost, the error starts decreasing. For a low number of nodal points (30) the quadratic elements seem to perform poorly in the vicinity of the inclusion (see Fig. 5d). As the number of elements increases, the quadratic elements improve rapidly, and when the response is calculated with 87 nodal points its performance is similar to that of the linear elements (see Fig. 7c and d).

Fig. 8 displays the analytical response and the BEM error when the vibrating source is excited with a frequency of 2450 Hz, and the number of the boundary elements used to model the inclusion satisfies the values of λ/L listed in Table 1, column R_3. Again, each plot results from computations performed with a similar number of nodal points, which is assumed to require similar computational cost. There are several interesting features to be noted in these results, which are strikingly different from the previous ones (i.e. those evaluated for a frequency of 2058.6 Hz). The constant elements now perform much better. However, the use of linear interpolating functions is still advantageous (see Fig. 8c).

The examples described depict the behavior of the BEM when a source with a specific frequency and wavenumber is

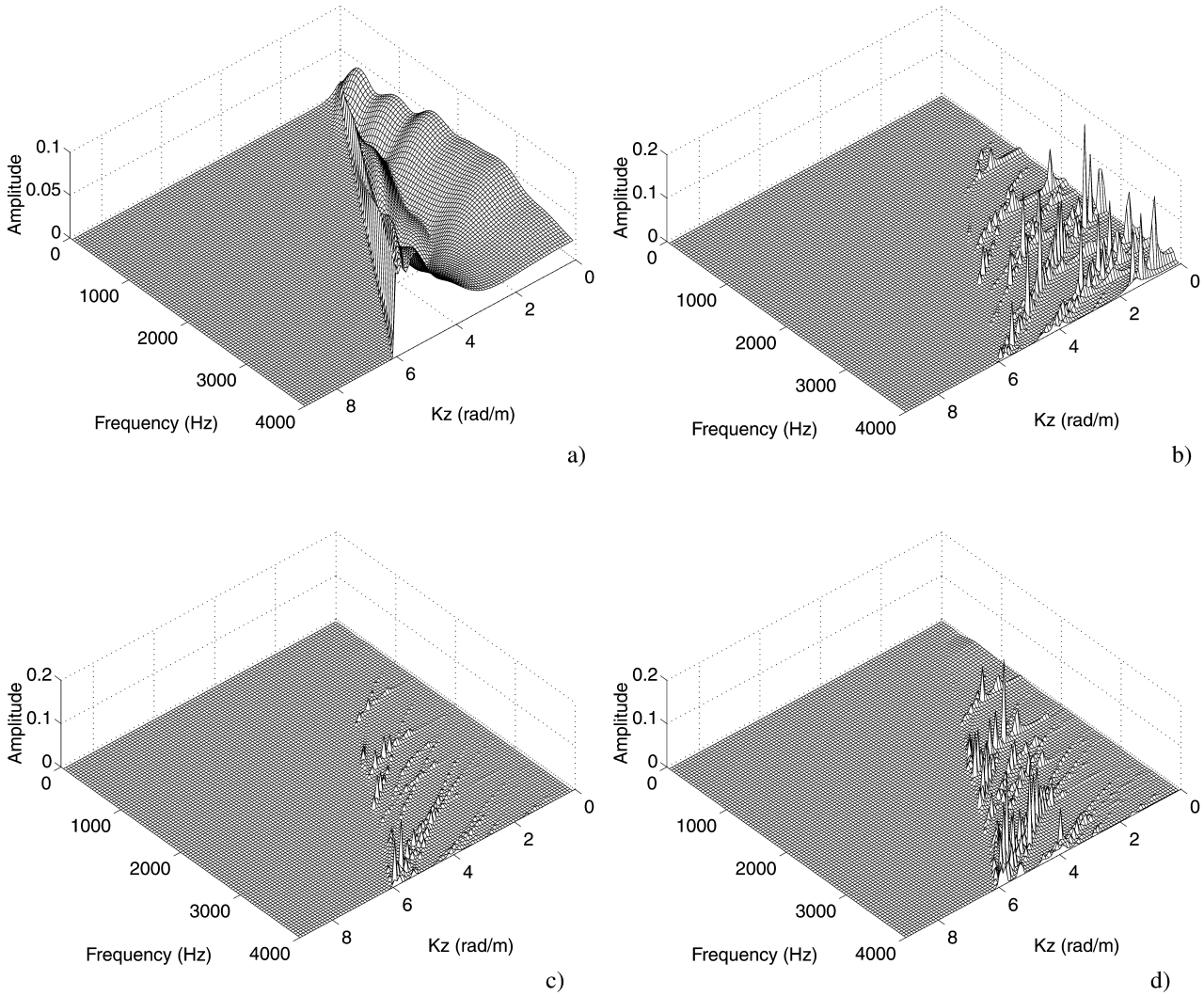

Fig. 10. Horizontal displacements at receiver 1 in the frequency versus wavenumber domain: (a) analytical solution; (b) modulus of the BEM error (R_3)—constant elements; (c) modulus of the BEM error (R_3)—discontinuous linear elements; and (d) modulus of the BEM error (R_3)—discontinuous quadratic elements.

excited. Indeed, as presented earlier, the 3D solution in frequency requires the calculation of a broad range of wavenumbers (see Eq. (4)), while the time solution additionally requires the response for a set of frequencies. To illustrate the performance of the BEM in the resolution of this problem, simulation analyses are next performed to calculate the full 3D response at receiver 1. Computations are performed in the frequency range (40–4000 Hz), with a frequency increment of 40 Hz. The spatial period considered in the analysis is $L = 2T\alpha = 210m$. The cavity is modeled with a number of boundary elements that changes with the frequency excitation of the harmonic load satisfying the ratios R_1 and R_3 (see Table 1). The minimum number of nodal points is kept at a minimum of 24. Fig. 9a displays the amplitude of the analytical horizontal displacement in the frequency versus wavenumber domain at receiver 1. Notice, that values of k_z in excess to ω/α correspond to inhomogeneous, evanescent waves which decay rapidly in space. The BEM errors, illustrated in Figs. 9b–d and 10b–d, when the relation λ/L assumes the values R_1 and R_3, respectively, have features similar to those observed in the previous cases. The position of the peak errors in these plots agrees with the solutions given by Eq. (A6), when the number of boundary elements increases. The quadratic elements perform poorly when the number of elements is defined by the ratio R_1 (see Fig. 9d). Again, the linear elements outperform constant and quadratic boundary elements, especially at low spatial wavenumbers (see Figs. 9c and 10c).

8. Position of nodal points inside linear and quadratic elements

In the above examples, the nodal points placed along the discontinuous elements were chosen to coincide with those

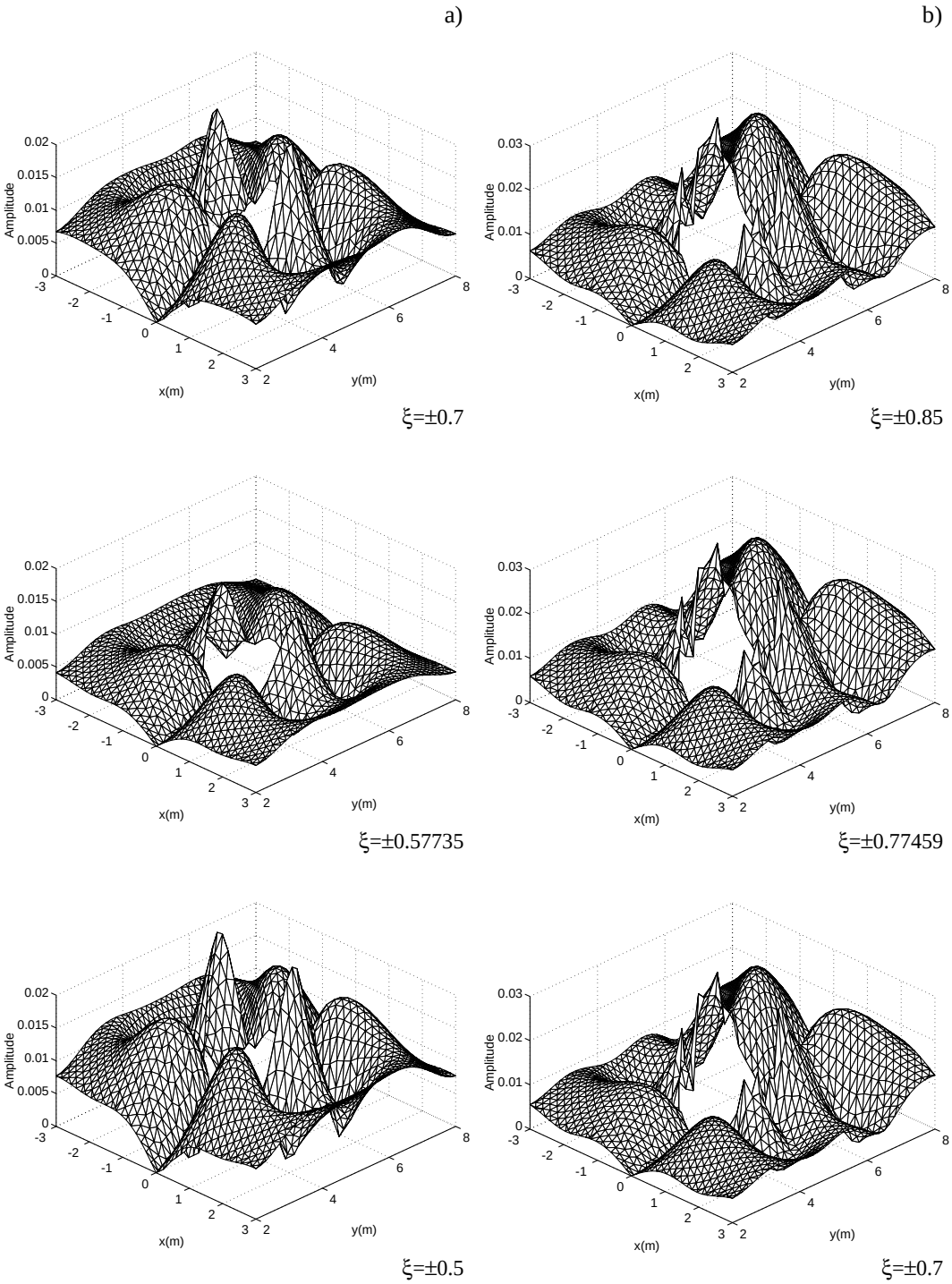

Fig. 11. Horizontal displacements ($k_z = 1$ rad/(m/s)). when the nodal points are placed at different positions inside of each element. Frequency of excitation—2058.6 Hz: (a) modulus of the BEM error (R_3)—discontinuous linear elements; (b) modulus of the BEM error (R_3)—discontinuous quadratic elements.

in a Gauss–Legendre numerical integration. Simulations performed using different positions for the nodal points suggest that this is a good choice. To demonstrate this assertion, consider the wave propagation problem described earlier. The scattered field is again computed for a cylindrical circular cavity over a fine grid placed around the inclusion. Fig. 11 displays the BEM error for the horizontal displacement for a frequency of 2058.6 Hz, and a relation of λ/L set to R_3 (see Table 1), for different locations of nodal points around those given by the Gauss–Legendre numerical integration, and when the inclusion is modeled with linear and quadratic elements,

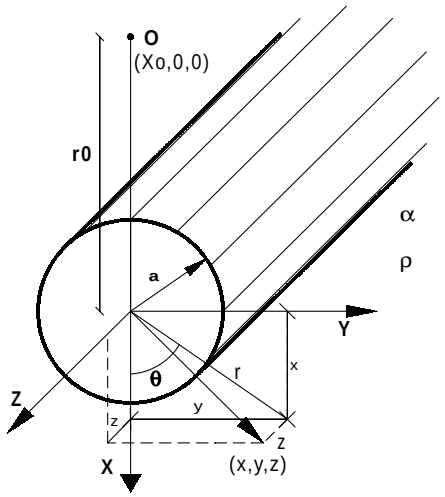

Fig. 12. Geometry of the problem.

respectively. In all the analyses, the interior nodal point of the quadratic elements is placed at the center of the boundary segment.

The accuracy obtained with the linear elements varies conspicuously with the position of the nodal points. It can be further observed that the solution improves as the nodal points are moved to the positions used in the Gauss–Legendre integration. The quadratic elements' results do not appear to be greatly affected when the nodal points are moved around the vicinity of the Gauss–Legendre numerical integration points. However, as the nodal points move to the extremity of the boundary element, the BEM solution clearly loses accuracy.

Simulation analysis performed when the source vibrates at 2450 Hz (not illustrated here) demonstrates similar behavior. The BEM error was subsequently tested for different sized cylindrical circular cavities, for a broad range of frequencies and spatial wavenumbers, which demonstrated similar conduct.

9. Conclusions

This paper evaluates the benefits gained by using discontinuous elements, (in which the nodal points are inside each element), to model 3D elastic environments with constant, linear and quadratic interpolation functions. Simulation analyses were performed using circular cylindrical models, namely, cavities. The number of boundary elements used changed according to the different relations between the wavelength (λ) of the incident waves and the length of the boundary elements (L).

Comparison of the BEM results with those obtained by analytical solution revealed the importance of using linear elements instead of constant and quadratic elements to calculate the displacement field. It has been illustrated that the linear boundary elements outperform the constant and quadratic elements, especially at frequencies in the vicinity of natural modes.

It was also observed that the position of the nodal points inside the linear elements significantly influences the accuracy of the displacement solution at frequencies in the vicinity of the natural modes of vibration. Locating the nodal points to coincide with the Gauss–Legendre numerical integration points was found to be a good choice.

Appendix A

This appendix presents in condensed form the closed-form solution to evaluate the 3D field generated by a dilatational point source in the presence of a circular cylindrical cavity of infinite length submerged in an elastic medium.

Consider a spatially uniform elastic medium of infinite extent, having a cylindrical cavity (Fig. 12). Decomposing the homogeneous wave equations for elastic media by means of the now classical dilatational potential ϕ and shear potentials ψ, χ, one is led to the three scalar wave equations in these potentials, with associated wave propagation velocities α, β, and β, respectively. For a harmonic dilatational point source at an off-center position $(x_0, 0, 0)$ that is oscillating with a frequency ω, the scalar wave equations go over into three Helmholtz equations whose solution can be expressed in terms of the single dilatational potential for the *incident* waves, together with a set of potentials for *scattered* waves in the elastic medium.

The incident dilatational potential, after being Fourier-transformed Eq. (A1) in the *z direction*, can be expressed by

$$\phi_{\text{inc}}(\omega, x, y, \kappa_z) = \frac{-\mathrm{i}A}{2} H_0^{(2)}(\kappa_\alpha \sqrt{(x - x_0)^2 + y^2}) \qquad \text{(A1)}$$

This equation can be written in terms of waves centered at the origin,

$$\phi_{\text{inc}}(\omega, r, \theta, \kappa_z) = -\frac{\mathrm{i}A}{2} \sum_{n=0}^{\infty} (-1)^n \epsilon_n H_n^{(2)}(\kappa_\alpha r_0) J_n(k_\alpha r) \cos n\theta$$

$$\text{when } r < r_0 \qquad \text{(A2)}$$

$$\phi_{\text{inc}}(\omega, r, \theta, \kappa_z) = -\frac{\mathrm{i}A}{2} \sum_{n=0}^{\infty} (-1)^n \epsilon_n H_n^{(2)}(\kappa_\alpha r) J_n(k_\alpha r_0) \cos n\theta$$

$$\text{when } r > r_0 \qquad \text{(A3)}$$

in which the $J_n^{(2)}(\ldots)$ are Bessel functions of order n, θ is the

azimuth, and

$$\epsilon_n = \begin{cases} \frac{1}{2} & \text{if n} = 0 \\ 1 & \text{if n} \neq 0 \end{cases} \quad \text{(A4)}$$

$r = \sqrt{x^2 + y^2}$ = radial distance to the receiver

$r_0 = \sqrt{x_0^2} = |x_0|$ = radial distance to the source

$\cos\theta = \text{x/r}, \sin\theta = \text{y/r}$

In the frequency-axial-wavenumber domain, the scattered field can be expressed in a form similar to that of the incident field, namely

$$\phi^s_{\text{sca}}(\omega, r, \theta, k_z) = \sum_{n=0}^{\infty} A_n H_n^{(2)}(k_\alpha r) \cos n\theta \quad \text{(A5)}$$

$$\psi^s_{\text{sca}}(\omega, r, \theta, k_z) = \sum_{n=0}^{\infty} B_n H_n^{(2)}(k_\beta r) \sin n\ \theta$$

$$\chi^s_{\text{sca}}(\omega, r, \theta, k_z) = \sum_{n=0}^{\infty} C_n H_n^{(2)}(k_\beta r) \cos n\ \theta$$

in which the subscript *sca* denotes the scattered field, A_n, B_n, and C_n, are as yet unknown coefficients to be determined from appropriate boundary conditions, namely $\sigma_{rr} = \sigma_{r\theta} = \sigma_{rz} = 0$, at $r = a$. The imposition of the three stated boundary conditions for each summation index n then leads to a system of three equations in the three unknown constants. Having obtained the constants, we may compute the motions associated with the scattered field by means of the well-known equations relating potentials and displacements.

Natural modes—The frequency and spatial wavenumber position of the natural modes are found to be important to how the BEM performs. The position of these natural modes can be evaluated, assuming that they are both incoming and outgoing cylindrical waves propagating to and from the center of the cylinder. Imposing the resulting boundary conditions, $u_r = u_\theta = u_z = 0$ at $r = a$, in the presence of this standing field, the response is other than zero if the following determinant is set to be zero. The solution of the resulting equation gives the required position of the natural modes.

$$\begin{vmatrix} d_{11} & d_{12} & d_{13} \\ d_{21} & d_{22} & d_{23} \\ d_{31} & d_{32} & d_{33} \end{vmatrix} = 0 \quad \text{(A6)}$$

where

$$d_{11} = \left[\frac{n}{a} J_n(\alpha_1 a) - \alpha_1 J_{n+1}(\alpha_1 a) \right]$$

$$d_{12} = \frac{n}{a} J_n(\beta_1 a)$$

$$d_{13} = -\text{i}k_z \left[\frac{n}{a} J_n(\beta_1 a) - \beta_1 J_{n+1}(\beta_1 a) \right]$$

$$d_{21} = -\frac{n}{a} J_n(\alpha_1 a)$$

$$d_{22} = \left[-\frac{n}{a} J_n(\beta_1 a) + \beta_1 J_{n+1}(\beta_1 a) \right]$$

$$d_{23} = \frac{n}{a}\ \text{i}k_z J_n(\beta_1 a)$$

$$d_{31} = -\text{i}k_z J_n(\alpha_1 a)$$

$$d_{32} = 0$$

$$d_{33} = \beta_1^2 J_n(\beta_1 a).$$

References

[1] Trifunac MD. Surface motion of a semi-cylindrical alluvial valley for incident plane SH waves. Bull Seismol Soc Am 1971;61:1755–70.

[2] Wong HL, Trifunac MD. Surface motion of semi-elliptical alluvial valley for incident plane SH-waves. Bull Seismol Soc Am 1974;64:1389–403.

[3] Lee VW. On deformations near circular underground cavity subjected to incident plane SH waves. Symposium of Application of Computer Methods in Engineering, University of Southern California, LA, USA, 1977. p. 951–61.

[4] Datta SK, Shah AH. Scattering of SH-waves by embedded cavities. Wave Motion 1982;4:265–83.

[5] Lee VW. Three-dimensional diffraction of elastic waves by a spherical cavity in an elastic half-space. 1: Closed-form solutions. Soil Dyn Earthq Engng 1988;7:149–61.

[6] Lee VW, Karl JA. Diffraction of SV waves by underground circular, cylindrical cavities. Soil Dyn Earthq Engng 1992;11:445–56.

[7] Sanchez-Sesma FJ. Diffraction of elastic waves by three dimensional surface irregularities. Bull Seismol Soc Am 1983;73:1621–36.

[8] Moeen-Vaziri N, Trifunac MD. Scattering and diffraction of plane P and SV waves by two-dimensional inhomogeneities: Part II. Soil Dyn Earthq Engng 1988;7:189–200.

[9] Lee VW, Wu X. Application of the weighted residual method to diffraction by 2-D canyons of arbitrary shape: II. Incident P, SV and Rayleigh waves. Soil Dyn Earthq Engng 1994;13:365–75.

[10] Waas G. Linear two-dimensional analysis of soil dynamics problems in semi-infinite layered media, PhD dissertation, University of California, Berkeley, CA, USA, 1972.

[11] Lysmer J, Udaka T, Seed HB, Hwang R. LUSH—A computer program for complex response analysis of soil-structure systems, report no. EERC 74-4, Earthquake Engineering Research Center, University of California, Berkeley, CA, USA, 1974.

[12] Kausel E. Forced vibrations of circular foundations in layered media, MIT research report 70-3, Department of Civil Engineering, Massachusetts Institute of Technology, Cambridge, MA, USA, 1974.

[13] Ohtsuki A, Harumi K. Effect of topography and subsurface inhomogeneities on seismic SV waves. Earthq Engng Struct Dyn 1983;11:441–62.

[14] Shah AH, Wong KC, Datta SK. Diffraction of plane SH waves in a half-space. Earthq Engng Struct Dyn 1982;10:519–28.

[15] Beskos DE. In: Manolis GD, Davies TG, editors. Wave propagation

through ground. Boundary element techniques in geomechanics, London: Computational Mech, 1993. p. 359–406.
[16] Sánchez-Sesma FJ, Campillo M. Topographic effects for incident P, SV and Rayleigh waves. Tectonophysics 1993;218:113–25.
[17] Wong HL. Effect of surface topography on the diffraction of P, SV, and Rayleigh waves. Bull Seismol Soc Am 1982;72:1167–83.
[18] Tadeu AJB, Kausel E, Vrettos C. Scattering of waves by subterranean structures via the boundary element method. Soil Dyn Earthq Engng 1996;15:387–97.
[19] Bouchon M, Aki K. Discrete wave-number representation of seismic-source wave field. Bull Seismol Soc Am 1977;67:259–77.
[20] Phinney RA. Theoretical calculation of the spectrum of first arrivals in layered elastic mediums. J Geophys Res 1965;70:5107–23.
[21] Tadeu AJB, Santos PFA. Scattering of waves by buried cavities via boundary element method. EUROBEM, Wessex Institute of Technology, Southampton, UK, 1998. p. 189–200.
[22] Santos P, Tadeu A. Scattering of waves by buried inclusions via boundary element method. Proceedings, XXV IAHS World Housing Congress, International Association for Housing Science, Lisbon, Portugal, 1998. p. 655–64.
[23] Manolis GD, Beskos DE. Boundary element methods in elastodynamics. London: Chapman and Hall, 1988.
[24] Brebbia CA, Telles JC, Wrobel LC. Boundary elements techniques. Theory and applications in engineering. Berlin: Springer, 1984.
[25] Pao YH, Mow CC. Diffraction of elastic waves and dynamic stress concentrations. New York: Crane and Russak, 1973.
[26] Tadeu AJB. Modeling and seismic imaging of buried structures, PhD thesis, M.I.T., Department of Civil Engineering, Cambridge, MA, USA, 1992.